

## Accepted Manuscript

Effect of baseplate positioning on fixation of reverse total shoulder arthroplasty

Min Zhang, Sarah Junaid, Thomas Gregory, Ulrich Hansen, Cheng-Kung Cheng



PII: S0268-0033(18)30773-3  
DOI: <https://doi.org/10.1016/j.clinbiomech.2018.12.021>  
Reference: JCLB 4671  
To appear in: *Clinical Biomechanics*  
Received date: 17 September 2018  
Accepted date: 20 December 2018

Please cite this article as: Min Zhang, Sarah Junaid, Thomas Gregory, Ulrich Hansen, Cheng-Kung Cheng, Effect of baseplate positioning on fixation of reverse total shoulder arthroplasty. *Jclb* (2018), <https://doi.org/10.1016/j.clinbiomech.2018.12.021>

This is a PDF file of an unedited manuscript that has been accepted for publication. As a service to our customers we are providing this early version of the manuscript. The manuscript will undergo copyediting, typesetting, and review of the resulting proof before it is published in its final form. Please note that during the production process errors may be discovered which could affect the content, and all legal disclaimers that apply to the journal pertain.

**Effect of Baseplate Positioning on Fixation of Reverse Total Shoulder Arthroplasty**

Min Zhang PhD<sup>1,2</sup>, Sarah Junaid PhD<sup>2,3</sup>, Thomas Gregory MD<sup>2,4</sup>, Ulrich Hansen PhD<sup>2</sup>,  
Cheng-Kung Cheng PhD<sup>1</sup>

<sup>1</sup> School of Biological Science and Medical Engineering, Beihang University, Beijing, China, 100083; Beijing Advanced Innovation Centre for Biomedical Engineering, Beihang University, Beijing, China, 102402.

<sup>2</sup> Mechanical Engineering Department, Imperial College London, UK.

<sup>3</sup> Engineering and Applied Sciences, Aston University, Birmingham, UK

<sup>4</sup> Department of Orthopaedic Surgery, Avicenne Teaching Hospital, APHP, University ParisXIII, Bobigny, France

Min Zhang: zhangminsky123@msn.com

Sarah Junaid: [s.junaid@aston.ac.uk](mailto:s.junaid@aston.ac.uk)

Thomas Gregory: [tms.gregory@gmail.com](mailto:tms.gregory@gmail.com)

Ulrich Hansen: [u.hansen@imperial.ac.uk](mailto:u.hansen@imperial.ac.uk)

Cheng-Kung Cheng: [ckcheng2009@gmail.com](mailto:ckcheng2009@gmail.com)

**Corresponding author:** Name: Min Zhang

E-mail address: zhangminsky123@msn.com

Mailing address: No. 37, Xueyuan Road, Haidian District,  
Beijing, China 100083

**Word count for abstract: 245; Word count for the main text: 3600**

**Declarations of interest: none**

**Abstract**

*Background:* The glenoid component in reverse total shoulder arthroplasty is recommended to be positioned inferiorly or with a downward tilt with the intention of reducing scapular notching. However, it is still unclear whether modifying the position of the glenoid prosthesis affects implant stability. The aim of this study was to determine the association between implant positioning and glenoid prosthesis fixation using Grammont reverse total shoulder arthroplasty.

*Methods:* Four positions for the glenoid prosthesis were studied using the finite element method. The glenosphere was positioned as follows: 1) in the middle of the glenoid fossa, 2) flush with the inferior glenoid rim, 3) with an inferior overhang, 4) with a 15° inferior inclination. Bone-prosthesis micromotions and strain-induced bone adaptations were quantified during five daily activities.

*Findings:* When the glenoid component was tilted inferiorly, the activities producing anterior-posterior shear forces (e.g. standing up from an armchair) caused an increase in peak micromotions. In the lateral-middle glenoid, inferior positioning caused a 64.6% reduction in bone apparent density. In the lateral-inferior glenoid, central positioning led to the most severe bone resorption, reaching 43.9%.

*Interpretation:* Reducing activities which generate anterior-posterior shear forces on the shoulder joint will increase bone formation and may improve the primary stability of the implant when fixed in the position with an inferior tilt. Postoperative bone resorption is highly dependent on implant positioning. Understanding the relationship between bone resorption and implant positioning will help surgeons improve the long-term stability of reverse total shoulder arthroplasty.

**Keywords** inferior position; inferior tilt; reverse total shoulder arthroplasty; bone remodeling; micromotion; fixation.

ACCEPTED MANUSCRIPT

## 1. Introduction

Loosening of the glenoid is a common complication for Grammont reverse total shoulder arthroplasty (RSA), with an incidence rate of 3.5% to 9%, and often requires reintervention (Zumstein et al., 2010; Boileau, 2016). In addition to infection, there are many other factors leading to aseptic glenoid loosening, i.e. scapular notching, osseointegration, and strain-induced bone loss (Pilliar et al., 1986; Huiskes et al., 1987; Chae et al., 2015; Boileau, 2016).

Scapular notching is caused by mechanical impingement between the humeral component and the scapular neck during arm adduction and is hastened by bone osteolysis. It is reported to be present in approximately 50% to 96% of Grammont RSA (Sirveaux et al., 2004; Simovitch et al., 2007; Kempton et al., 2011). Inferior positioning and inferior tilting are recommended to minimise postoperative scapular notching in RSA (Nyffeler et al., 2005; Kelly II et al., 2008). The space between the glenoid bone and the inferior rim of the glenoid component is generally recommended to be maintained within the range of 2 mm to 6 mm (Kelly II et al., 2008; Kontaxis and Johnson, 2009; Kempton et al., 2011). The recommended angle of inclination is between 10° and 15° (Nyffeler et al., 2005; Kempton et al., 2011).

Osseointegration is the direct structural and functional connection between living bone and the surface of a load-bearing implant. Pilliar reported that the occurrence of bone ingrowth is closely correlated with the relative movement between the bone and the implant, which is also known as micromotion (Pilliar et al., 1986). Bone ingrowth occurs in the presence of micromotion within a threshold of 50  $\mu\text{m}$  (Pilliar et al., 1986). However, when bone-implant micromotion exceeds 150  $\mu\text{m}$ , mature fibrous connective tissues form a less stable connection with the implant (Pilliar et al., 1986). Finite element method has been used to calculate bone-prosthesis micromotion after RSA, and then to predict the occurrence of

postoperative integration utilizing the relationship between micromotion and bone ingrowth (Chae et al., 2016).

Stress-shielding is another factor leading to erosion of the bone bed supporting the RSA (Ahir and Walker, 2004). Finite element analysis has been used extensively for predicting stress distribution and strain-induced bone remodelling (Büchler et al., 2002; Sharma et al., 2009; Sharma et al., 2010; Suárez et al., 2012). Suárez (2012) evaluated the effects of the assumption of bonding and unbonding conditions at the bone-prosthesis interface on bone adaptation in a finite element model. Sharma (2010) reported on the correlation between strain-induced bone adaptation and the design of total shoulder prostheses.

Even though inferior positioning and inferior tilting have been proposed for minimizing scapular notching (Boileau, 2017), it is still unclear how this may affect bone ingrowth and bone adaptation during normal daily activities. It hypothesizes that the placement of glenoid component will relate to the implant fixation. This study is aimed to investigate the hypothesis using finite element analysis.

## 2. Methods

### 2.1 Finite element (FE) modelling

CT images (Voxel sizes:  $0.48\text{mm} \times 0.48\text{mm} \times 0.33\text{mm}$ ) of a 71-year-old cadaveric scapula without any previous shoulder surgeries and disease (Science Care, Phoenix, USA) were used to create the geometry of the bone in Avizo 5 (Mercury Systems, Andover, USA). The geometry of a Delta CTA RSA (Depuy Synthes Company, Warsaw, USA) was inserted into the bone model according to the recommended surgical techniques for a Delta CTA implant (2005 version) (Depuy Synthes Company, Warsaw, USA). Four positions of the glenoid component were simulated (Fig. 1): (a) glenoid prosthesis fixed in the middle of the glenoid fossa (FP1), (b) glenoid prosthesis positioned flush to the glenoid rim (FP2), (c) glenoid component moved inferiorly until the inferior locking screw protruded from the bone (FP3), (d) glenoid component inclined inferiorly by approximately  $15^\circ$  (FP4) (Nyffeler et al., 2005). With a fixed angle of  $17^\circ$  from the inferior surgical screw to the middle peg of the implant, the distance between the bottom of the glenosphere and the inferior rim of the glenoid bone for FP3 was 3.9 mm, which is within the reported range of overhang of the glenoid component (2 to 4 mm) for a Delta CTA RSA (Nyffeler et al., 2005). With the intersection of the superoinferior and anteroposterior axes being a reference point (Nyffeler et al., 2005), determination of the entry point of the central peg for the four implant positions (Fig. 1) was 0 mm for FP1, 0.8 mm inferiorly for FP2, 4.7 mm inferiorly for FP3 and 0 mm for FP4. Inclinations for the four prosthesis positions (Fig. 1) were  $0^\circ$ (FP1),  $0^\circ$ (FP2),  $0^\circ$ (FP3) and  $15^\circ$ (FP4) respectively. In the FP4 model, the downward tilt of the glenoid implant required resection of the inferior glenoid pole. All the glenoid positions were guided by an experienced orthopaedic shoulder surgeon. For each placement, geometries of the scapula and the implant were imported into FE software. In this study, MSC. Marc Mentat (MSC Software Corporation, Santa Ana, USA) was utilized for creating resected surface on the

glenoid, meshing and FE analysis. All models were constructed from linear tetrahedral elements and assumed to be linearly elastic and isotropic. The material properties of bone in each FE model were calculated using the relationship introduced by Carter and Hays (1977) and were assigned element-by-element. The FE model of the scapula was validated against the cadaveric scapula in our previous work (Zhang, 2012). The glenoid head and baseplate of the implant, which are manufactured from cobalt-chrome, were modeled as linear isotropic materials with a Young's modulus of 220 GPa. The four titanium screws used to secure the implant were modeled as linear isotropic materials with a Young's modulus of 110 GPa.

The baseplate of the Delta CTA RSA was press-fit to the bone. To evaluate micromotion at the bone-baseplate interface, the baseplate in the FE model was assumed to be unbounded and set with a frictional surface-to-surface contact with the bone. 0.4 was recommended for the friction coefficient at the baseplate-bone interface (Harman et al., 2005; Hopkins et al., 2008). In addition, varying the coefficient of friction was found not significantly affect the predicted micromotions in our previous work (Zhang, 2012). In this current study, the four peripheral surgical screws in the RSA were assumed to be securely tightened. Thus, the interface between bone and screws was modelled as a rigidly bonded interface. Five physiological activities from daily life were simulated: 1) Combing hair, 2) Lifting a block higher than the shoulders, 3) Lifting a block to shoulder height, 4) Hands on the lower back, 5) Sit-to-stand from an armchair (Supplementary) (Kontaxis, 2010). Force magnitudes (Supplementary (d) (e)) and loading positions (Supplementary (f) (g)) in each activity were obtained from Kontaxis' study, as well as the scapular reference coordinate (Kontaxis, 2010). In the intact bone model (Supplementary (b)), AI represents the inferior angle, AA is the posterior point of the acromion, and TS is the medial end of the scapular spine. The origin of the coordinate system in the FE model of the intact bone is on the point AA; Xs is on the line determined by AA and TS; Ys is vertical to Xs; Zs is vertical to the plane determined by AA,

TS and AI; The coordinate system of the implanted scapula was defined based on the resected surface (Supplementary (c)). The origin of the coordinate system in the FE model of the implanted scapula is on the middle point of the baseplate. X is vertical to the resected surface, Y is from the inferior to the superior, Z is from the posterior to the anterior. The medial ends of the scapula in each FE model were fixed to prevent movement and so as not to influence the motion of the glenoid. Bone-implant micromotions and strain-induced bone resorption were recorded for various fixation positions. The quality of the meshes was checked using a mesh convergence study, finding that a mesh size of 1.5 mm in the lateral scapula and 3.0 mm in the remaining bone offered a reliable prediction of interface micromotion and bone adaptation.

## 2.2 Micromotion analysis

The relative displacement of each pair of contacting nodes on the fixation interface after loading was calculated. This indicated the extent of micromotion of that pair of nodes. The micromotion of all the nodes at the bone-implant interface in each physiological activities shown in the supplementary (Kontaxis, 2010) was recorded for each implant position. The calculation method was validated by Harman and Hopkins (Harman et al., 2005; Hopkins et al., 2008). Our previous study investigated micromotion and post-operative stress variations in six FE models of cadaveric scapulae implanted with a Delta CTA RSA in the middle of the glenoid (Zhang, 2012). The results showed the same level of micromotion and bone density distribution across all models. Thus, this study used one of the scapulae for analyzing micromotion and bone remodelling with the Delta CTA RSA fixed in various positions.

## 2.3 Bone adaptation analysis

The strain-induced bone remodelling algorithm proposed by Weinans et al. was used in this study (Weinans et al., 1992). This algorithm was developed in accordance with 'Wolff's

Law' and uses strain energy density as the feedback. It has been clinically validated using the adaptation of periprosthetic human bone by Kerner et al. (Kerner et al., 1999). For the purpose of investigating changes in bone density in this current study, only the internal structure was remodelled and the outer shape of the glenoid was assumed to be unchanged. Changes in bone apparent density were calculated on an element-by-element basis and expressed by Equation 1.

$$\begin{aligned} \Delta\rho^i &= \tau \Delta t A(\rho^i) \{S^i - S_n^i(1+s)\}, & S^i &\geq S_n^i(1+s) \\ &= \tau \Delta t A(\rho^i) \{S^i - S_n^i(1-s)\}, & S^i &\leq S_n^i(1-s) \end{aligned} \quad \text{Equation 1}$$

$$(0 \text{ g/cm}^3 < \rho < 1.8 \text{ g/cm}^3)$$

Where  $i$  relates to elements,  $S$  is the bone remodelling stimulus ( $S = U / \rho$ ),  $U$  is the strain energy density,  $S_n$  is the reference stimulus,  $\tau$  is the time scale (the relationship between simulated time and real time),  $A(\rho)$  is the free surface density (Martin, 1984),  $\Delta t$  is the time increment expressed in Equation 2, and  $s$  is a constant for determining the extent of the stimulus range. In this study,  $s=0.75$  was used (Kerner et al., 1999), as this value has been successfully validated with in-vitro tests by Kerner et al. (1999) and Bitsakos (2005). The reference stimulus ( $S_n = U_n / \rho_n$ ) was calculated according to the strain energy ( $U_n$ ) and bone apparent density ( $\rho_n$ ), which were obtained from an intact scapula bone. Five physiological daily activities were applied to the intact scapula (Supplementary) (Kontaxis, 2010). The stimulus was calculated for each loading condition and the average of the stimuli from all loading conditions represented the stimulus ( $S$ ) in one iteration. In each iteration, the Young's modulus was calculated using the relationship proposed by Carter and Hayes (1977) and was updated when the next iteration started. The Poisson's ratio was assumed to be constant during the entire bone adaption process.

$$\tau \Delta t = \frac{\Delta\rho_{max}}{\{A(\rho)(S - (1+s)S_n)\}_{max}} \quad \text{Equation 2}$$

Variations in distribution of bone apparent density in the frontal plane, which passes through the middle of the stem, were recorded and used to predict postoperative adaptive bone resorption in the scapula.

Five regions of interest were chosen for statistical comparison of glenoid positioning (Fig. 2). Three regions were in the lateral glenoid and two regions were in the medial glenoid (Fig. 2). The bone apparent density in each region was averaged. A student's t-test was applied to investigate the relationship between the position of the glenoid implant and strain-induced bone adaptation. A *P* value of less than 0.05 was considered significant.

### 3. Results

Micromotion at the bone-prosthesis interface was recorded for the four glenoid implant positions under five loading conditions (Tasks 1 to 5) (Supplementary). The interface micromotion while standing up from an armchair (Task 5) was illustrated in Fig. 3. The results indicate that large interface micromotions were predominantly located at the tip of the central peg, as well as at the superior and inferior rims of the baseplate. In comparison with the other three positions, an inferior tilt of the glenoid prosthesis led to a considerable increase in micromotion at the inferior region of the baseplate.

The maximum micromotion at the bone-prosthesis interface for each implant position (Fig. 1) under the five loading conditions (tasks 1 to 5) (Supplementary) is illustrated in Fig. 4. It was found that the maximum micromotion in FP4 (inferior tilt of the glenoid implant) reached 82.5  $\mu\text{m}$  in Task 2 (Lifting a block to head height) and 137.4  $\mu\text{m}$  in Task 5 (Standing up from an armchair). In Task 5, where the greatest micromotion was observed across all activities, micromotion of less than 50  $\mu\text{m}$  (the threshold value for bone ingrowth) covered 73.5% of the baseplate. For the implant positions without any inferior tilting, the average peak micromotion for the five loading conditions (Supplementary) was 27.4  $\mu\text{m}$  for FP1, 25.2  $\mu\text{m}$  for FP2 and 26.6  $\mu\text{m}$  for FP3. However, for Task 5 alone, the peak micromotion reached 67.2  $\mu\text{m}$  for FP1, 63.5  $\mu\text{m}$  for FP2 and 65.4  $\mu\text{m}$  for FP3.

Variations in the distribution of postoperative bone apparent density with time for the four glenoid implant positions were predicted with a bone remodelling algorithm. Results at four follow up stages are shown in Fig. 5. It was found that severe bone resorption occurred around the central peg and the back of the baseplate in all four models. Low apparent densities predominantly appeared above the central peg when the glenoid component was

located inferiorly (FP2 and FP3) and were distributed almost evenly around the central peg in FP1 and FP4.

The percentage change in mean bone apparent density in the postoperative period of F4 in the five regions of interest is shown in Fig. 6. It is noticeable that the bone apparent density at the lateral-middle (2) region showed high strain-induced bone resorption for FP2 (64.1% (SD 9.7%)) and FP3 (64.6% (SD 9.5%)). There were no lateral-middle values in the case of central positioning of the glenoid (FP1 and FP4), as this region just covered the hole for the implant stem. In the lateral-inferior region (3), central positioning of the glenoid component (FP1: 43.9% (SD 17.1%) and FP4: 43.8% (SD 19.8%)) led to greater variation in bone apparent density than moving the glenoid component inferiorly (FP2: 25.9% (SD 21.1%) ( $p<0.05$ ) and FP3: 25.0% (SD 16.7%) ( $p<0.05$ )). In addition, Fig. 6 also illustrates a greater reduction in bone apparent density in the lateral region (1, 2, 3) than in the medial region (4, 5).

#### 4. Discussion

This study simulated implantation of the glenoid components of an RSA in four different positions to analyse micromotion at the bone-prosthesis interface and bone adaptation. The most important findings were that (1) inferior tilting of the glenoid component lead to high levels of micromotion in the inferior glenoid, but this is activity-specific, and (2) postoperative bone resorption is highly dependent on implant positioning.

The micromotion detailed in Fig. 4 shows that inferior positioning (FP3) of the implant did not result in different levels of micromotion than could be expected with a traditional implant position (FP1). For the positions with 0° tilt, the average peak micromotion for all the loading conditions (27.4  $\mu\text{m}$  in FP1, 25.2  $\mu\text{m}$  in FP2 and 26.6  $\mu\text{m}$  in FP3) was lower than the upper limit of 50  $\mu\text{m}$ , above which bone formation would not occur (Pilliar et al., 1986). This indicated a suitable initial stability of the glenoid prosthesis. This finding is consistent with radiological reports for successful RSAs (Roche et al., 2013; Boileau, 2016). Variations in peak micromotions for the different activities show that a patient's lifestyle may affect the initial stability of the implant. The high peak micromotions observed for Task 5 (67.2  $\mu\text{m}$  in FP1, 63.5  $\mu\text{m}$  in FP2 and 65.4  $\mu\text{m}$  in FP3) indicates that further studies into the relationship between lifestyle and micromotion could be beneficial for developing improved guidelines for postoperative recovery.

Tilting the glenoid component inferiorly led to an increase in peak micromotions. Noticeably, the value was 82.5  $\mu\text{m}$  in Task 2 (lifting a block to head height) and 137.4  $\mu\text{m}$  in Task 5 (standing up from an armchair). This suggests that bone ingrowth would not occur in the inferior part of the glenoid because both values exceeded the upper limit of 50  $\mu\text{m}$  for stimulating bone formation (Pilliar et al., 1986). Roberts et al. reported similar findings in an anteroposterior radiographic study, where serious inferior radiolucent lines were observed

with the use of an inferior-tilt configuration (Roberts et al., 2007). Using in-vitro testing and finite element simulations, Chae et al. also reported high micromotion in the inferior part of the glenoid (Chae et al., 2015; Chae et al., 2016). The greatest micromotion was observed in Task 5. However, micromotion below 50  $\mu\text{m}$  covered 73.5% of the baseplate. This explains the initial stability of the glenoid component when fixed with an inferior tilt (Simovitch et al., 2007). Variations in peak micromotion for position FP4 (inferior titling of baseplate) for the five loading conditions (Task 1: 16.1  $\mu\text{m}$ , Task 2: 82.5  $\mu\text{m}$ , Task 3: 19.8  $\mu\text{m}$ , Task 4: 12.3  $\mu\text{m}$ , Task 5: 137.4  $\mu\text{m}$ ) showed that the increase in micromotion induced by glenoid positioning is activity-specific. Reducing activities that produce high anterior-posterior shear forces (for example, Task 2 & 5) may improve the primary stability of the prosthesis when fixed with an inferior tilt.

In comparison to positioning with a  $0^\circ$  inclination, tilting the implant inferiorly induced a superior shift in the glenohumeral resultant force on the glenosphere surface and increased bone loss around the inferior glenoid pole. The magnitude of the resultant glenohumeral (GH) force, which originates from the muscles surrounding the shoulder, is assumed not to be related to implant positioning. Changing the position of the loading point may reduce the shear forces on the implant and thus was not a factor for the increase of micromotions in FP4. Tilting the implant required the inferior scapular pole to be resected, leading to increased contact between trabecular bone and the implant. This weak bone supporting the implant may explain the high micromotions in the inferior region observed in our study (Chae et al., 2015). An inferior inclination of the glenosphere requires the removal of cortical bone, which has been suggested to increase the risk of glenoid loosening (James et al., 2011; Kempton et al., 2011; Roche et al., 2013). In addition, specific recommendations for reducing scapular notching by tilting the glenosphere are still controversial (Edwards et al., 2012; Li et al., 2013).

Bone density distributions in the frontal plane for four glenoid positions under various loading conditions were predicted in this study. The results indicated the same tendency for strain-induced bone resorption in all four implant positions. Bone loss occurred initially in the area next to the bone-prosthesis interface, and then expanded to the peripheral regions. This finding is consistent with radiographic observations of bone loss in Grammont RSA (Roberts et al., 2007; Fávvaro et al., 2015).

This study also demonstrated that changing the position of the glenoid prosthesis induced different levels of strain-induced bone resorption. An inferior movement of the glenoid component led to greater bone resorption in the lateral-middle region, while central positioning of the glenoid component induced increased bone loss in the lateral-inferior region. These observations are corroborated by radiographic images (Roberts et al., 2007; Farshad and Gerber, 2010; Fávvaro et al., 2015). Farshad et al. reported that radiographic bone resorption at eight years after RSA was more severe than at three years, with the most noticeable region being above the central peg (Farshad and Gerber, 2010). The distribution of bone resorption with inferior positioning of the glenoid prosthesis in RSA is possibly caused by the inferior movement of the glenohumeral force on the glenoid bone. The inferior movement was 1.8 mm for FP2 and 3.9 mm for FP3 . Thus the load above the middle peg (lateral-middle region) after implantation reduced significantly, leading to low postoperative strains and greater bone resorption.

A limitation of this study is that the time constant used in the strain-induced bone remodelling algorithm has only been validated in studies on hip replacements for dogs (Kerner et al., 1999; Bitsakos, 2005). It is necessary to develop a time constant which could connect the predicted bone remodelling with clinical data obtained from patients with RSA. It would be beneficial to assess bone resorption in real time with different glenoid positions. Another limitation is that the bone-baseplate interface was assumed to be unbonded, which is

a worst case scenario. In a study evaluating the effect of various connection conditions at the bone-baseplate interface on the amount of bone resorption, Suárez et al. reported that bonding the interface (best case scenario) produced slightly less bone resorption than when the interface was unbonded (worst case scenario) (Suárez et al., 2012). This current study evaluated the amount of bone resorption when the glenoid component was fixed in various positions. Changing the position of the implant will lead to the same effects on results as long as the bone-baseplate interface connection conditions in the various FE models are the same.

ACCEPTED MANUSCRIPT

## 5. Conclusions

In conclusion, tilting the glenoid component inferiorly would lead to increased micromotion in the inferior glenoid, but the amount of micromotion depends on the activity being performed. Reducing activities with anterior-posterior shear forces will improve the primary stability of the bone-prosthesis interface when the prosthesis is fixed with an inferior tilt. Moving the glenoid component inferiorly led to a reduction in bone apparent density in the lateral-middle region. Central positioning of the glenoid component increased bone resorption in the lateral-inferior glenoid. Understanding the relationship between postoperative bone resorption and implant positioning is beneficial for improving the long-term stability of RSA.

**Acknowledgement**

We wish to thank Dr. Kontaxis from Newcastle University for the provision of force data for Delta reverse total shoulder arthroplasty in physiological daily activities. We would also like to thank Dr. Denny Lie, Singapore General Hospital, for helpful discussions on the standard surgical technique for Delta CTA reverse total shoulder arthroplasty.

ACCEPTED MANUSCRIPT

**Conflict of interest statement**

All the authors, their immediate family, and any research foundation with which they are affiliated have not received any financial payments or other benefits from any commercial entity related to the subject of this article.

ACCEPTED MANUSCRIPT

**References**

1. Ahir, S.P., Walker, P.S., 2004. Analysis of glenoid fixation for a reversed anatomy fixed-fulcrum shoulder replacement. *J Biomech* 37, 1699-1708, doi: 10.1016/j.jbiomech.2004.01.031.
2. Bitsakos, C., 2005. Computer Simulation of Periprosthetic Bone Remodelling after Total Hip Arthroplasty. PhD. thesis, Imperial College London, London, UK.
3. Boileau, P., 2016. Complications and revision of reverse total shoulder arthroplasty. *Orthop Traumatol Surg Res* 102, S33-S43, doi: 10.1016/j.otsr.2015.06.031.
4. Boileau, P., Morin-Salvo, N., Gauci, M., Seeto, B., Chalmers, P., Holzer, N., Walch, G., 2017. Angled BIO-RSA (bony-increased offset-reverse shoulder arthroplasty): a solution for the management of glenoid bone loss and erosion. *J Shoulder Elbow Surg* 26, 2133-2142, doi: 10.1016/j.jse.2017.05.024.
5. Büchler, P., Ramaniraka, N., Rakotomanana, L., Iannotti, J., Farron, A., 2002. A finite element model of the shoulder: application to the comparison of normal and osteoarthritic joints. *Clin Biomech* 17, 630-639, doi: [https://doi.org/10.1016/S0268-0033\(02\)00106-7](https://doi.org/10.1016/S0268-0033(02)00106-7).
6. Carter, D.R., Hayes, W.C., 1977. The compressive behaviour of bone as a two-phase porous structure. *J Bone Joint Surg Am* 59, 954-962, doi: <https://insights.ovid.com/pubmed?pmid=561786>.
7. Chae, S., Lee, J., Han, S., Kim, S., 2015. Inferior tilt fixation of the glenoid component in reverse total shoulder arthroplasty: A biomechanical study. *Orthop Traumatol Surg Res* 101, 421-425, doi: 10.1016/j.otsr.2015.03.009.
8. Chae, S.W., Lee, H., Kim, S.M., Lee, J., Han, S.H., Kim, S.Y., 2016. Primary stability of inferior tilt fixation of the glenoid component in reverse total shoulder arthroplasty: A finite element study. *J Orthop Res* 34, 1061-1068, doi: 10.1002/jor.23115.

9. Edwards, T.B., Trappey, G.J., Riley, C., O Connor, D.P., Elkousy, H.A., Gartsman, G.M., 2012. Inferior tilt of the glenoid component does not decrease scapular notching in reverse shoulder arthroplasty: results of a prospective randomized study. *J Shoulder Elbow Surg* 21, 641-646, doi: 10.1016/j.jse.2011.08.057.
10. Farshad, M., Gerber, C., 2010. Reverse total shoulder arthroplasty--from the most to the least common complication. *Int Orthop* 34, 1075-1082, doi: 10.1007/s00264-010-1125-2.
11. Fávaro, R.C., Abdulahad, M., Filho, S.M., Valério, R., Superti, M.J., 2015. Rotator cuff arthropathy: what functional results can be expected from reverse arthroplasty? *Rev Bras Ortop* 50, 523-529, doi: 10.1016/j.rbo.2015.04.007.
12. Harman, M., Frankle, M., Vasey, M., Banks, S., 2005. Initial glenoid component fixation in "reverse" total shoulder arthroplasty-A biomechanical evaluation. *J Shoulder Elbow Surg* 14, 162S-167S, doi: 10.1016/j.jse.2004.09.030.
13. Hopkins, A.R., Hansen, U.N., Bull, A.M.J., Emery, R., Amis, A., 2008. Fixation of the reversed shoulder prosthesis. *J Biomech* 17, 974-980, doi: 10.1016/j.jse.2008.04.012.
14. Huiskes, R., Weinans, H., Grootenboer, H.J., Dalstra, M., Fudala, B., Slooff, T.J., 1987. Adaptive bone-remodeling theory applied to prosthetic-design analysis. *J Biomech* 20, 1135-1150, doi: 10.1016/0021-9290(87)90030-3.
15. James, J., Huffman, K.R., Werner, F.W., Sutton, L.G., Nanavati, V.N., 2011. Does glenoid baseplate geometry affect its fixation in reverse shoulder arthroplasty? *J Shoulder Elbow Surg* 21, 917-924, doi: 10.1016/j.jse.2011.04.017.
16. Kelly II, J.D., Humphrey, C.S., Norris, T.R., 2008. Optimizing glenosphere position and fixation in reverse shoulder arthroplasty, Part One: The twelve-mm rule. *J Shoulder Elbow Surg* 17, 589-594, doi: 10.1016/j.jse.2007.08.013.

17. Kempton, L.B., Balasubramaniam, M., Ankerson, E., Wiater, J.M., 2011. A radiographic analysis of the effects of glenosphere position on scapular notching following reverse total shoulder arthroplasty. *J Shoulder Elbow Surg* 20, 968-974, doi: 10.1016/j.jse.2010.11.026.
18. Kerner, J., Huiskes, R., van Lenthe, G.H., Weinans, H., van Rietbergen, B., Engh, C.A., Amis, A.A., 1999. Correlation between pre-operative periprosthetic bone density and post-operative bone loss in THA can be explained by strain-adaptive remodelling. *J Biomech* 32, 695-703, doi: 10.1016/S0021-9290(99)00041-X.
19. Kontaxis, A., Johnson, G.R., 2009. The biomechanics of reverse anatomy shoulder replacement - A modelling study. *Clin Biomech* 24, 254-260, doi: 10.1016/j.clinbiomech.2008.12.004.
20. Kontaxis, A., 2010. Biomechanical analysis of reverse anatomy shoulder prosthesis. PhD. thesis, Newcastle University, Newcastle UK.
21. Li, X., Knutson, Z., Choi, D., Lobatto, D., Lipman, J., Craig, E.V., Warren, R.F., Gulotta, L.V., 2013. Effects of glenosphere positioning on impingement-free internal and external rotation after reverse total shoulder arthroplasty. *J Shoulder Elbow Surg* 22, 807-813, doi: 10.1016/j.jse.2012.07.013.
22. Martin, R.B., 1984. Porosity and specific surface of bone. *CRC Critical Reviews Biomed. Engng.* 10, 179-222, doi: <https://www.ncbi.nlm.nih.gov/pubmed/6368124>.
23. Nyffeler, R.W., Werner, C.M.L., Gerber, C., 2005. Biomechanical relevance of glenoid component positioning in the reverse Delta III total shoulder prosthesis. *J Shoulder Elbow Surg* 14, 524-528, doi: 10.1016/j.jse.2004.09.010.
24. Pilliar, R.M., Lee, J.M., Maniopoulos, C., 1986. Observations on the effect of movement on bone ingrowth into porous-surfaced implants. *Clin Orthop Relat Res* 208, 108-113, doi: <https://www.ncbi.nlm.nih.gov/pubmed/3720113>.

25. Roberts, C.C., Ekelund, A.L., Renfree, K.J., Liu, P.T., Chew, F.S., 2007. Radiologic assessment of reverse shoulder arthroplasty. *Radiographics* 27, 223-235, doi: 10.1148/rg.271065076.
26. Roche, C.P., Diep, P., Hamilton, M., Crosby, L.A., Flurin, P.H., Wright, T.W., Zuckerman, J.D., Routman, H.D., 2013. Impact of inferior glenoid tilt, humeral retroversion, bone grafting, and design parameters on muscle length and deltoid wrapping in reverse shoulder arthroplasty. *Bull Hosp Joint Dis* 71, 284-293, doi: <http://presentationgrafix.com/dev/cake/files/archive/pdfs/66.pdf>.
27. Roche, C.P., Marczuk, Y., Wright, T.W., Flurin, P.H., Grey, S., Jones, R., Routman, H.D., Gilot, G., Zuckerman, J.D., 2013. Scapular notching and osteophyte formation after reverse shoulder replacement. *Bone Joint J* 95, 530-535, doi: 10.1302/0301-620X.95B4.30442.
28. Sharma, G.B., Debski, R.E., McMahon, P.J., Robertson, D.D., 2009. Adaptive glenoid bone remodeling simulation. *J Biomech* 42, 1460-8, doi: 10.1016/j.jbiomech.2009.04.002.
29. Sharma, G.B., Debski, R.E., McMahon, P.J., Robertson, D.D., 2010. Effect of glenoid prosthesis design on glenoid bone remodeling: adaptive finite element based simulation. *J Biomech* 43, 1653-1659, doi: 10.1016/j.jbiomech.2010.03.004.
30. Simovitch, R.W., Zumstein, M.A., Lohri, E., Helmy, N., Gerber, C., 2007. Predictors of scapular notching in patients managed with the Delta III reverse total shoulder replacement. *J Bone Joint Surg Am* 89(3), 588-600, doi: 10.2106/JBJS.F.00226.
31. Sirveaux, F., Favard, L., Oudet, D., Huquet, D., Walch, G., Mole, D., 2004. Gammont inverted total shoulder arthroplasty in the treatment of glenohumeral osteoarthritis with massive rupture of the cuff: Results of a multicentre study of 80 shoulders. *Bone Joint J* 86, 388-395, doi: 10.1302/0301-620X.86B3.14024.

32. Suárez, D.R., Weinans, H., van Keulen, F., 2012. Bone remodelling around a cementless glenoid component. *Biomech Model Mechanobiol* 11, 903-913, doi: 10.1007/s10237-011-0360-9.
33. Weinans, H., Huiskes, R., Grootenboer, H.J., 1992. The behavior of adaptive bone-remodeling simulation models. *J Biomech* 25, 1425-41, doi: 10.1016/0021-9290(92)90056-7.
34. Zhang, M., 2012. Effects of Scapular Notching and Bone Remodelling on Long-Term Fixation of the Glenoid Component in Reverse Shoulder Arthroplasty. PhD. thesis, Imperial College London, London, UK.
35. Zumstein, M.A., Pinedo, M., Old, J., Boileau, P., 2010. Problems, complications, reoperations, and revisions in reverse total shoulder arthroplasty: a systematic review. *J Shoulder Elbow Surg* 20, 146-157, doi: 10.1016/j.jse.2010.08.001.

## Author contributions

Name of Author	Contribution (CRediT roles)
Min Zhang	Conceptualization; Data curation; Formal analysis; Investigation; Methodology; Project administration; Validation
Sarah Junaid	Validation
Thomas Gregory	Clinical support
Ulrich Hansen	Supervision
Cheng-Kung Cheng	Supervision

**Conflict of interest statement**

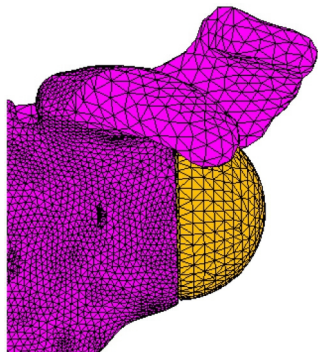
All the authors, their immediate family, and any research foundation with which they are affiliated have not received any financial payments or other benefits from any commercial entity related to the subject of this article.

ACCEPTED MANUSCRIPT

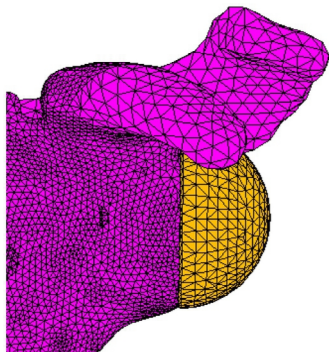
**Highlights**

- Inferior tilting of implant leads to increased micromotion in the inferior glenoid
- The amount of micromotion is activity-specific
- Reducing activities with anteroposterior shear forces improves implant stability
- Inferior positioning increases bone resorption in the lateral-middle glenoid
- Central positioning increases bone resorption in the lateral-inferior region

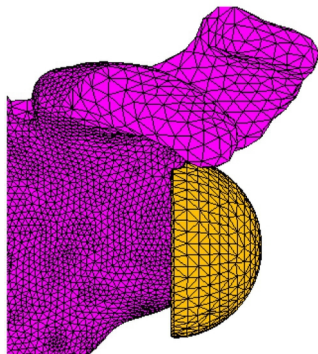
ACCEPTED MANUSCRIPT



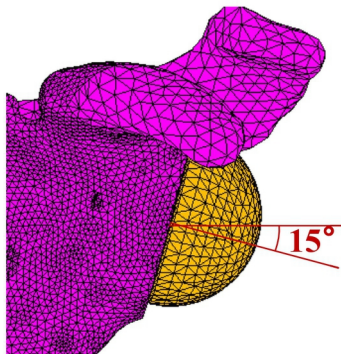
**FP1**  
(a)



**FP2**  
(b)

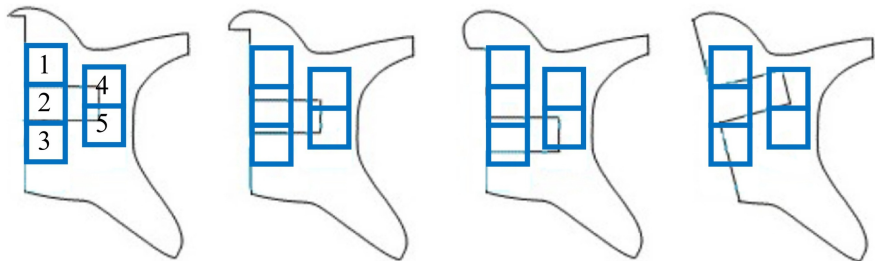


**FP3**  
(c)



**FP4**  
(d)

Figure 1



1 - Lateral superior; 2 - Lateral middle; 3 - Lateral inferior;  
4 - Medial superior; 5 - Medial inferior

Figure 2

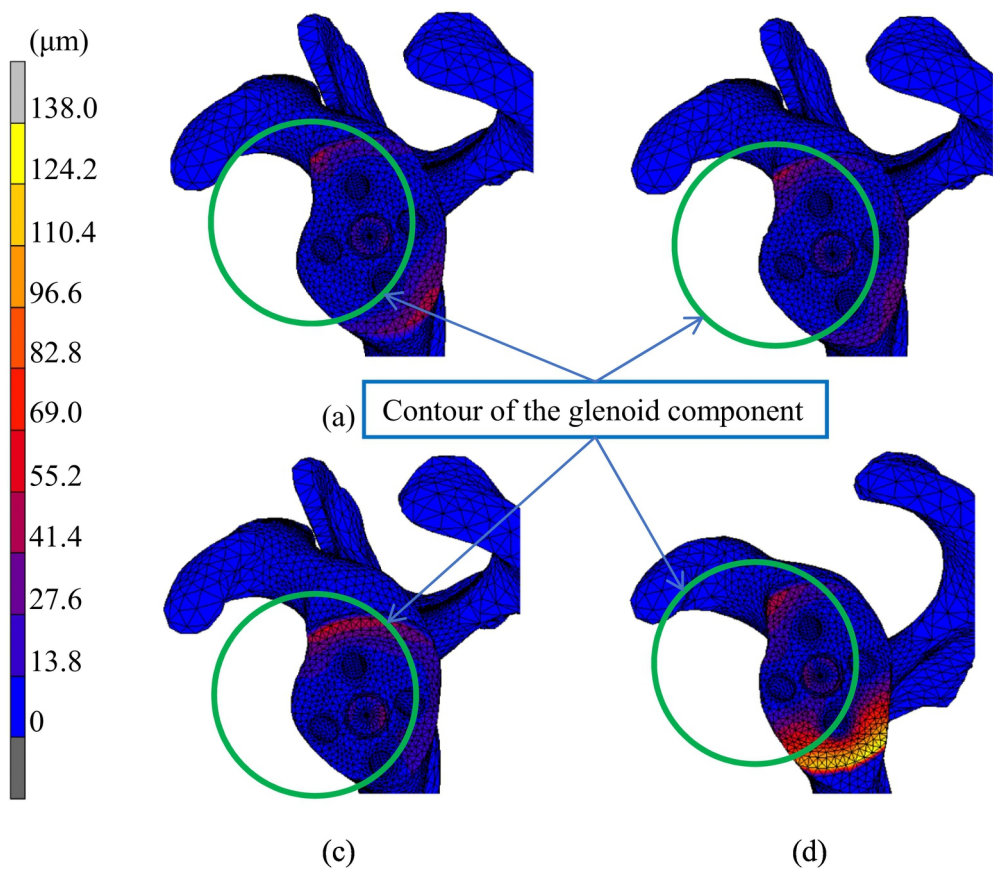
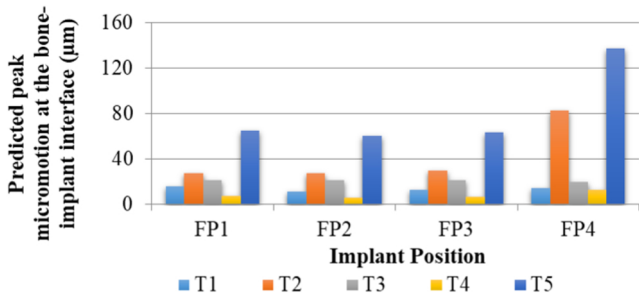


Figure 3



T1 - Combing hair; T2 - Lifting a block to head height;  
 T3 - Lifting a block to shoulder height; T4 - Hands on the  
 lower back; T5 - Sit-to-stand from an armchair

Figure 4

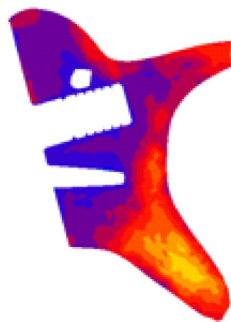
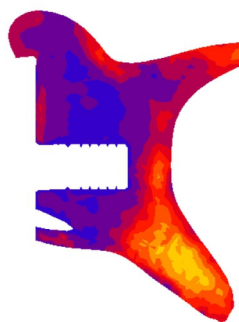
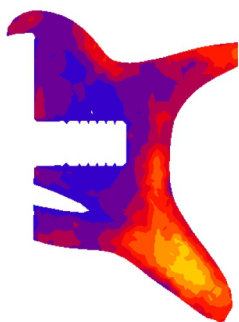
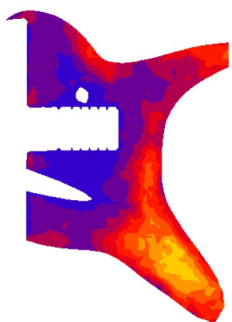
FP1

FP2

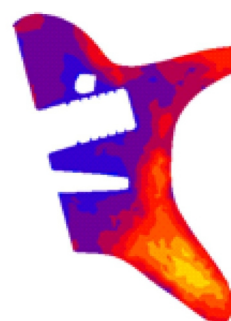
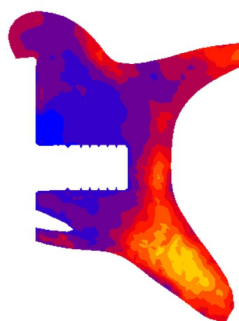
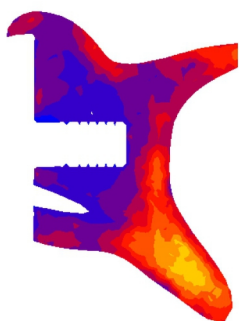
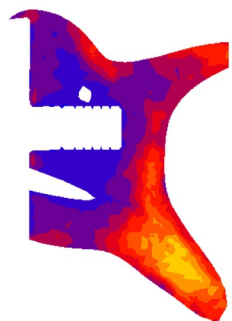
FP3

FP4

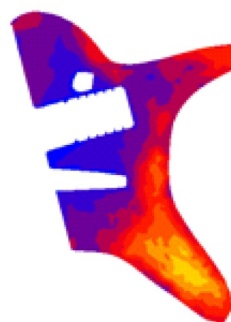
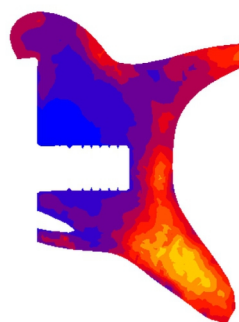
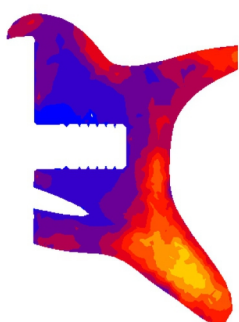
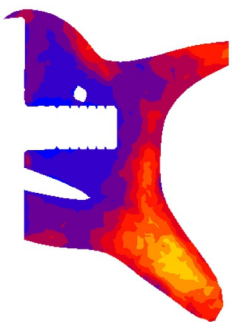
F0



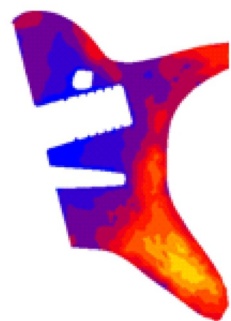
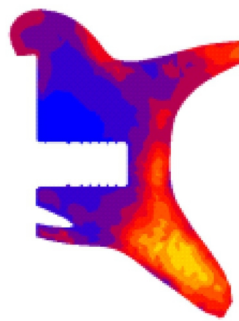
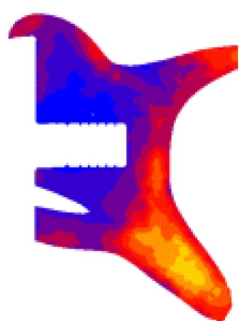
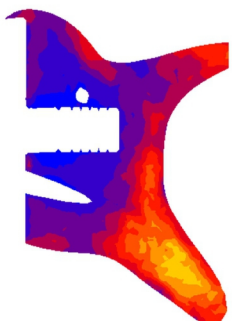
F1



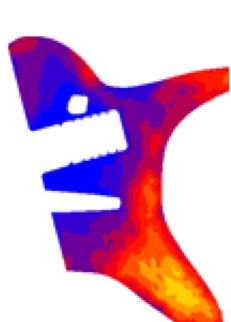
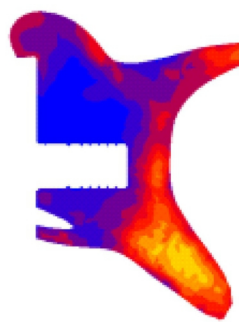
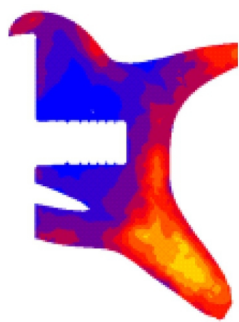
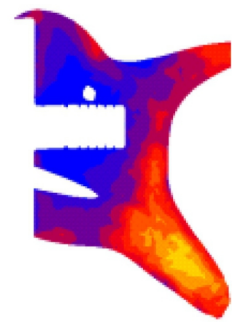
F2



F3

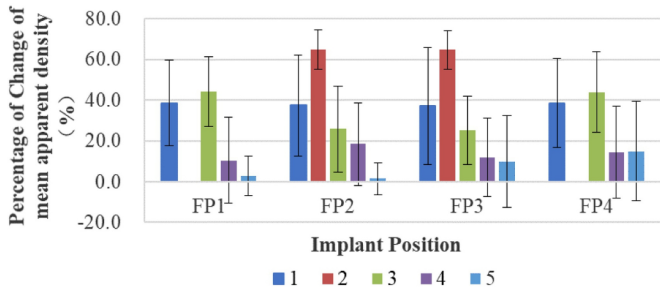


F4

 $(\text{g}/\text{cm}^3)$ 

1.80 1.62 1.44 1.26 1.08 0.90 0.72 0.54 0.36 0.18 0

Figure 5



1 - Lateral superior; 2 - Lateral middle; 3 - Lateral inferior;  
4 - Medial superior; 5 - Medial inferior

Figure 6